A MIXED SPECTRAL FINITE-DIFFERENCE MODEL FOR NEUTRALLY STRATIFIED BOUNDARY-LAYER FLOW OVER ROUGHNESS CHANGES AND TOPOGRAPHY

A. C. M. BELJAARS*, J. L. WALMSLEY, and P. A. TAYLOR

Boundary-Layer Research Division, Atmospheric Environment Service, 4905 Dufferin Street, Downsview, Ontario, Canada M3H 5T4

(Received in final form 24 November, 1986)

Abstract. A linear model for neutral surface-layer flow over complex terrain is presented. The spectral approach in the two horizontal coordinates and the finite-difference method in the vertical combines the simplicity and computational efficiency of linear methods with flexibility for closure schemes of finite-difference methods. This model makes it possible to make high-resolution computations for an arbitrary distribution of surface roughness and topography. Mixing-length closure as well as $E - \varepsilon$ closure are applied to two-dimensional flow above sinusoidal variations in surface roughness, the step-in-roughness problem, and to two-dimensional flow over simple sinusoidal topography. The main difference between the two closure schemes is found in the shear-stress results. $E - \varepsilon$ has a more realistic description of the memory effects in length and velocity scales when the surface conditions change. Comparison between three-dimensional model calculations and field data from Askervein hill shows that in the outer layer, the advection effects in the shear stress itself are also important. In this layer, an extra equation for the shear stress is needed.

1. Introduction

The atmospheric boundary layer above homogeneous terrain has been the subject of many studies and is reasonably well documented (see, for example, the workshop edited by Nieuwstadt and van Dop, 1982). Real terrain, however, is seldom uniform; surface inhomogeneities range from varying surface roughness and temperature to topographic effects. This paper deals with neutral surface-layer flow over an arbitrary roughness and height distribution with horizontal scales up to 10×10 km.

Several investigations have been devoted to idealised configurations. A classic example is the step-in-roughness problem which has been studied experimentally (Antonia and Luxton, 1971; Bradley, 1968) and by means of different turbulence models (Panofsky and Townsend, 1964; Townsend, 1965; Taylor, 1969; Peterson, 1969b; Rao *et al.*, 1974; see also Hunt and Simpson, 1982 for a review). Jackson and Hunt (1975) developed a linear two-dimensional theory for flow perturbations induced by hills of low aspect ratio. This theory has been extended to three dimensions by Mason and Sykes (1979). The main feature of the theory is the distinction between an outer layer where the flow is pressure driven and an inner layer where the turbulent stresses play a role. In both layers, a constant advection velocity is assumed which enables analytic solution. The theory as presented by Mason and Sykes (1979) and Jackson and Hunt (1975) has

* Permanent affiliation: Royal Netherlands Meteorological Institute, P.O. Box 201, 3730 AE De Bilt, The Netherlands.

Boundary-Layer Meteorology **38** (1987) 273–303.

been the basis of a series of models developed by Walmsley *et al.* (1982, 1986) and Taylor *et al.* (1983). We shall refer to the operational version of these models as MS3DJH. Linear equations are used for the velocity perturbations and solved analytically in wavenumber space.

The main advantages of the MS3DJH model are that it can deal very easily with arbitrary distributions of terrain roughness and elevation and that the computer requirements for memory and process time are very low, even for high-resolution runs. The surface height map is Fourier transformed, the solution for each wavenumber is calculated individually and the solution is inverse-transformed to real space. Disadvantages of this method are the limitation to small perturbations, the approximation of the advection velocity by a constant and the mixing-length closure. The linear approximation, however, turns out to allow quite large perturbations in both terrain elevation and roughness and is probably adequate in many applications. The main limitations of MS3DJH are the approximation of the advection terms and, especially, the level of closure. Replacing the mixing-length approximation by more sophisticated closure results in a set of equations that we have not been able to solve analytically.

It has been shown in many studies that in neutral inhomogeneous boundary-layer flow, the velocity changes are quite insensitive to the closure scheme (see Hunt and Simpson, 1982; also Taylor *et al.*, 1985 for a review). This means that the mixing-length approximation is usually adequate if we are interested in the velocity profiles only. The turbulence characteristics, however, depend very much on the closure scheme. As shown by Peterson (1969a), Rao *et al.* (1974), and Beljaars *et al.* (1983), equilibrium between production and dissipation rate of turbulent energy, which is necessary for mixing-length closure, is seldom found in the case of changing surface roughness. Topographic perturbations also produce non-equilibrium effects which cannot be dealt with by simple mixing-length closure (Zeman and Jensen, 1985). In the present paper, we shall show some results with mixing-length closure but we shall also develop a model using $E - \varepsilon$ closure ($k - \varepsilon$ in the engineering literature). Details will be given later.

Since the equations are too complex for analytic solutions, we have to solve them numerically. It is felt, however, that for moderately complex terrain, the linear approximation of the equations as in MS3DJH (see Walmsley *et al.*, 1986) results in only minor errors except perhaps on the lee side of a hill. The linear approach has the advantage that it results in a very simple treatment of arbitrary boundary conditions and that, as will be shown later, wavenumber-dependent scaling can be applied. The latter means that the vertical gridspacing is adapted to the penetration depth of the perturbation. This mechanism certainly contributes to the accuracy of the solution with minimal computational costs.

In this paper, we describe a Mixed Spectral Finite-Difference Model (referred to as MSFD). The equations are linearized around the upstream or other representative unperturbed profile and Fourier-transformed in the two horizontal coordinates. The resulting set of ordinary differential equations in the vertical coordinate is solved by means of a finite-difference technique.

The model is described in Section 2. Two closure schemes are applied: the standard

mixing-length closure and the $E - \varepsilon$ closure. In Section 3, results will be shown for a sinusoidal perturbation in the logarithm of the surface roughness and for the step-in-roughness problem. Section 4 deals with flow over sinusoidal topography. In Section 5, the model is applied to the real topography of Askervein hill, for which experimental data are available. It is shown that in the outer layer, an extra equation is needed in order to arrive at realistic predictions of the shear stress.

2. Description of the Model

2.1. The continuity and momentum equations

We start with the Reynolds equations for steady incompressible flow where the boundary-layer approximation is applied to the stress terms:

$$\begin{aligned} u\frac{\partial u}{\partial x} + v\frac{\partial u}{\partial y} + w\frac{\partial u}{\partial z} &= -\frac{1}{\rho}\frac{\partial p}{\partial x} + \frac{\partial \tau_x}{\partial z}\,, \\ u\frac{\partial v}{\partial x} + v\frac{\partial v}{\partial y} + w\frac{\partial v}{\partial z} &= -\frac{1}{\rho}\frac{\partial p}{\partial y} + \frac{\partial \tau_y}{\partial z}\,, \\ u\frac{\partial w}{\partial x} + v\frac{\partial w}{\partial y} + w\frac{\partial w}{\partial z} &= -\frac{1}{\rho}\frac{\partial p}{\partial z}\,, \\ \frac{\partial u}{\partial x} + \frac{\partial v}{\partial y} + \frac{\partial w}{\partial z} &= 0\,. \end{aligned} \tag{1}$$

In these equations, u, v, and w are wind components in the horizontal (x, y) and vertical (z) coordinates, respectively; p is pressure; τ_x and τ_y are the horizontal shear-stress components in the x- and y-direction and ρ is density (assumed constant in these computations).

In order to facilitate solution in cases with surface height changes, we transform to terrain-following coordinates with $f_1(x, y)$ as the height of the surface above a reference level:

$$X = x\,, \qquad Y = y\,, \qquad Z = z - f_1(x, y)\,. \tag{2}$$

The horizontal velocity components, stresses and pressure are split into an unperturbed part and a small perturbation (see also Walmsley *et al.*, 1982):

$$\begin{aligned} &u = u_0(Z) + u_1(X, Y, Z)\,, \qquad v = v_0(Z) + v_1(X, Y, Z)\,, \\ &\tau_x = \tau_{x0} + \tau_{x1}\,, \qquad \tau_y = \tau_{y0} + \tau_{y1}\,, \qquad p = p_0 + p_1\,. \end{aligned} \tag{3}$$

A corresponding representation for vertical velocity is:

$$w = u_0(Z)\,\partial f_1/\partial X + v_0(Z)\,\partial f_1/\partial Y + w_1(X, Y, Z)\,. \tag{3a}$$

The first-order perturbations can be due to both topographical influences and roughness changes. Since the perturbations are assumed to be small, the two contributions can simply be added. Equations for the first-order perturbations are found by substitution of (2) and (3) into (1) and neglecting the higher-order terms. It should be noted that $\partial f_1/\partial X$ and $\partial f_1/\partial Y$ are first-order terms and are assumed to be small. This means that hills are assumed to have a gentle slope rather than low height (see also Walmsley *et al.*, 1982). The first-order equations read:

$$
\begin{aligned}
&u_0 \frac{\partial u_1}{\partial X} + v_0 \frac{\partial u_1}{\partial Y} + w_1 \frac{\mathrm{d}u_0}{\mathrm{d}Z} = -\frac{1}{\rho}\frac{\partial p_1}{\partial X} + \frac{\partial \tau_{x1}}{\partial Z}\,, \\
&u_0 \frac{\partial v_1}{\partial X} + v_0 \frac{\partial v_1}{\partial Y} + w_1 \frac{\mathrm{d}v_0}{\mathrm{d}Z} = -\frac{1}{\rho}\frac{\partial p_1}{\partial Y} + \frac{\partial \tau_{y1}}{\partial Z}\,, \\
&u_0 \frac{\partial w_1}{\partial X} + v_0 \frac{\partial w_1}{\partial Y} + \left(u_0 \frac{\partial}{\partial X} + v_0 \frac{\partial}{\partial Y}\right)^2 f_1 = -\frac{1}{\rho}\frac{\partial p_1}{\partial Z}\,, \\
&\frac{\partial u_1}{\partial X} + \frac{\partial v_1}{\partial Y} + \frac{\partial w_1}{\partial Z} = 0\,.
\end{aligned}
\tag{4}
$$

Fourier transformation is carried out with, for example,

$$
\hat{u}_1(k, m) = \frac{1}{2\pi} \int_{-\infty}^{\infty}\int u_1(X, Y)\, e^{-ikX - imY}\, \mathrm{d}X\, \mathrm{d}Y\,, \tag{5}
$$

where k and m represent the horizontal wavenumbers and the caret symbol indicates the Fourier-transformed quantity. The transformed equations are:

$$
\begin{aligned}
&(iku_0 + imv_0)\hat{u}_1 + \frac{\mathrm{d}u_0}{\mathrm{d}Z}\,\hat{w}_1 = -\frac{1}{\rho}\, ik\hat{p}_1 + \frac{\partial \hat{\tau}_{x1}}{\partial Z}\,, \\
&(iku_0 + imv_0)\hat{v}_1 + \frac{\mathrm{d}v_0}{\mathrm{d}Z}\,\hat{w}_1 = -\frac{1}{\rho}\, im\hat{p}_1 + \frac{\partial \hat{\tau}_{y1}}{\partial Z}\,, \\
&(iku_0 + imv_0)\hat{w}_1 - (ku_0 + mv_0)^2 \hat{f}_1 = -\frac{1}{\rho}\frac{\partial \hat{p}_1}{\partial Z}\,, \\
&ik\hat{u}_1 + im\hat{v}_1 + \frac{\partial \hat{w}_1}{\partial Z} = 0\,.
\end{aligned}
\tag{6}
$$

In principle, any profile of the unperturbed velocity (u_0, v_0) could be used as long as it is compatible with the closure assumption. Here, however, we shall limit our analysis to cases with the usual logarithmic profile for the neutral surface layer, formulated with

$u_0 = v_0 = 0$ on $Z = 0$. This has:

$$u_0 = (u_*/\kappa)(\cos\phi)\ln[(Z + z_0)/z_0)]\,,$$
$$v_0 = (u_*/\kappa)(\sin\phi)\ln[(Z + z_0)/z_0)]\,, \tag{7}$$

where $\kappa = 0.4$ is Von Karman's constant, z_0 represents the roughness length appropriate to the undisturbed flow (and independent of x and y), u_* is the friction velocity, and ϕ is the angle of the unperturbed wind with respect to the x-axis. Although the equations may be simplified by choosing ϕ equal to 0, from a practical point of view it is more convenient to fix the input maps of topography and roughness with respect to the coordinates and to choose ϕ as an input parameter of the model.

2.2. Mixing-length closure

A very simple closure assumption is the mixing-length approximation where the stress is proportional to the velocity gradient and the exchange coefficient is proportional to a length scale (κZ) and a velocity scale $(\tau_x^2 + \tau_y^2)^{1/4}$. For an arbitrary wind direction the mixing-length closure is:

$$\tau_x = \kappa(Z + z_0)(\tau_x^2 + \tau_y^2)^{1/4}\frac{\partial u}{\partial Z}\,,$$
$$\tau_y = \kappa(Z + z_0)(\tau_x^2 + \tau_y^2)^{1/4}\frac{\partial v}{\partial Z}\,. \tag{8}$$

Note that, as a length scale, we have used $\kappa(Z + z_0)$, where z_0 is the roughness length corresponding to the undisturbed flow. For flow over topography only, with uniform surface roughness, this use is compatible with $u = v = 0$ at $Z = 0$ and can be applied for all Z; for flows over nonuniform surface roughness, $z_{01}(x, y)$, it is a valid approximation only for $Z \gg z_0, z_{01}$. In our treatment of the equations in cases with nonuniform roughness, we shall make use of the concept of a 'constant-flux' or 'wall' layer of depth $Z_w \gg z_0, z_{01}$. For $Z > Z_w$, we shall apply (8) while for $Z < Z_w$ we shall assume forms for the profiles which are compatible with the local surface roughness, z_{01}. This will be discussed in more detail in Section 2.4.

After substitution of (3), omission of second-order terms and Fourier transformation, we obtain

$$\hat{\tau}_{x1} = \kappa(Z + z_0)u_*\frac{\partial \hat{u}_1}{\partial Z} + \frac{1}{2}(\hat{\tau}_{x1}\cos\phi + \hat{\tau}_{y1}\sin\phi)\cos\phi\,,$$
$$\hat{\tau}_{y1} = \kappa(Z + z_0)u_*\frac{\partial \hat{v}_1}{\partial Z} + \frac{1}{2}(\hat{\tau}_{x1}\cos\phi + \hat{\tau}_{y1}\sin\phi)\sin\phi\,. \tag{9}$$

2.3. $E - \varepsilon$ closure

As noted earlier, it appears clear that the simple mixing-length approximation is not valid for turbulence computations in inhomogeneous flow. The advected turbulence remem-

bers the upstream conditions and adjusts only slowly to a new equilibrium. One way of simulating this is by applying differential equations for all second-order moments (see Mellor and Yamada, 1974, 1982; or Zeman, 1981 for a review). Slightly simpler models are, however, adequate in many cases; examples are given by Mellor and Yamada (1982). Quite a popular procedure is to express the fluxes proportional to gradients with the exchange coefficient dependent on velocity and length scales, calculated from differential equations. The most obvious choice for the velocity scale is the square root of the turbulent kinetic energy. With the velocity scale specified, there are a number of possibilities for the length scale. The length scale can be specified explicitly (Peterson, 1969b), a differential equation can be used for the length scale (Mellor and Yamada, 1982) or a dissipation-rate equation can be formulated (Lumley and Khajeh-Nouri, 1974). This is done in most second-order models, especially in engineering applications (see Durst *et al.*, 1979). Recently the $E - \varepsilon$ approach has been applied to atmospheric flow by Detering and Etling (1985) and by Caneill *et al.* (1985).

The $E - \varepsilon$ closure has the following form for neutral surface-layer flow:

$$\tau_x = K \frac{\partial u}{\partial z}, \qquad \tau_y = K \frac{\partial v}{\partial z}, \tag{10}$$

$$K = \frac{(\alpha E)^2}{\varepsilon}, \tag{11}$$

$$u \frac{\partial E}{\partial x} + v \frac{\partial E}{\partial y} + w \frac{\partial E}{\partial z} = P - \varepsilon + \frac{\partial}{\partial z}\left(\frac{K}{C_{KE}} \frac{\partial E}{\partial z}\right), \tag{12}$$

$$u \frac{\partial \varepsilon}{\partial x} + v \frac{\partial \varepsilon}{\partial y} + w \frac{\partial \varepsilon}{\partial z} = (C_{\varepsilon 1} P - C_{\varepsilon 2} \varepsilon) \frac{\varepsilon}{E} + \frac{\partial}{\partial z}\left(\frac{K}{C_{K\varepsilon}} \frac{\partial \varepsilon}{\partial z}\right), \tag{13}$$

where

$$P = \tau_x \frac{\partial u}{\partial z} + \tau_y \frac{\partial v}{\partial z},$$

is the production rate,

$$E = \tfrac{1}{2}(\overline{u'^2} + \overline{v'^2} + \overline{w'^2}),$$

is the turbulent kinetic energy, ε is the dissipation rate, and K is the exchange coefficient. It has been assumed that the diffusion coefficients for energy and dissipation rate are proportional to the one for momentum. A number of unknown parameters appear in these equations; they have to be determined empirically. Launder (1975) recommends $\alpha = 0.3$, $C_{\varepsilon 1} = 1.44$, $C_{\varepsilon 2} = 1.92$, $C_{KE} = 1$, and $C_{K\varepsilon} = 1.3$. These values, however, cannot be applied to atmospheric flow directly. Parameter α, which is the ratio of shear stress to kinetic energy for the homogeneous boundary layer, is different in the atmosphere. According to Panofsky and Dutton (1984), $\alpha = 0.18$ seems to be an appropriate value

for the atmosphere. Parameter $C_{\varepsilon 2}$ determines the destruction of dissipation rate and is usually chosen to fit the decay rate of isotropic turbulence. Since the value of this parameter has a clear physical basis, there seems to be little reason for changing it. One of two remaining parameters ($C_{\varepsilon 1}$ and $C_{K\varepsilon}$) in the ε-equation has to obey a constraint resulting from knowledge about the logarithmic profile in case of homogeneous flow. It can easily be shown that the following relation has to be satisfied (Launder, 1975):

$$C_{\varepsilon 2} - C_{\varepsilon 1} = \frac{\kappa^2}{\alpha C_{K\varepsilon}} \,. \tag{14}$$

For the remaining parameters C_{KE} and either $C_{\varepsilon 1}$ or $C_{K\varepsilon}$, we have to rely on comparison of the model results with data. Launder (1975) proposes $C_{KE} = 1$, which means that turbulent energy has the same diffusion coefficient as momentum. We have no reason to change this, particularly since the model results are quite insensitive to the value of C_{KE}. In engineering flows, the value of $C_{\varepsilon 1}$ is often adjusted to arrive at the right spreading rate for the round or plane jet. To reproduce measured profiles in the atmosphere, Detering and Etling (1985) had to specify a profile for $C_{\varepsilon 1}$. Since we are dealing with the neutral surface layer where the turbulence is shear-dominated, we feel that the engineering value, which is adjusted for thin shear layers, should be adequate. In future, however, it might be necessary to tune $C_{\varepsilon 1}$ in connection with data for inhomogeneous surface-layer flow. To make a proper choice for $C_{\varepsilon 1}$, detailed turbulence measurements are necessary; these are presently lacking for inhomogeneous flow. The parameters that are actually used in this study are:

$$\begin{aligned} &\alpha = 0.18\,, \qquad C_{\varepsilon 1} = 1.44\,, \qquad C_{\varepsilon 2} = 1.92\,, \\ &C_{KE} = 1\,, \qquad C_{K\varepsilon} = 1.85\,. \end{aligned} \tag{15}$$

In the framework of MSFD, we transform to (X, Y, Z) coordinates, separate E and ε into an upstream part and a perturbation, substitute the upstream profiles and do the Fourier transformation. The resulting equations for E_1 and ε_1 are:

$$\begin{aligned} (iku_0 + imv_0)\hat{E}_1 = {} & \frac{2u_*}{\kappa(Z + z_0)} \left(-\alpha \hat{E}_1 + \hat{\tau}_{x1} \cos\phi + \hat{\tau}_{y1} \sin\phi \right) \\ & + \frac{\partial}{\partial Z}\left[\frac{\kappa(Z + z_0)u_*}{C_{KE}} \frac{\partial \hat{E}_1}{\partial Z} \right], \end{aligned} \tag{16}$$

$$\begin{aligned} (iku_0 + imv_0)\hat{\varepsilon}_1 = {} & \frac{u_*^3}{\kappa(Z + z_0)^2} \hat{w}_1 + (C_{\varepsilon 1} - C_{\varepsilon 2}) \frac{2\alpha u_*}{\kappa(Z + z_0)} \hat{\varepsilon}_1 \\ & - (3C_{\varepsilon 1} - C_{\varepsilon 2}) \frac{\alpha^2 u_*^2}{\kappa^2(Z + z_0)^2} \hat{E}_1 + C_{\varepsilon 1} \frac{2\alpha u_*^2}{\kappa^2(Z + z_0)^2} (\hat{\tau}_{x1} \cos\phi + \hat{\tau}_{y1} \sin\phi) \\ & + \frac{1}{C_{K\varepsilon}} \frac{\partial}{\partial Z}\left[\kappa(Z + z_0)u_* \frac{\partial \hat{\varepsilon}_1}{\partial Z} - \frac{2\alpha u_*^2}{Z + z_0} \hat{E}_1 + \kappa u_* \hat{\varepsilon}_1 \right], \end{aligned} \tag{17}$$

$$\hat{\tau}_{x1} = \kappa(Z + z_0)u_* \frac{\partial \hat{u}_1}{\partial Z} + \cos\phi\left[2\alpha\hat{E}_1 - \frac{\kappa(Z + z_0)}{u_*}\hat{\varepsilon}_1\right],$$
$$\hat{\tau}_{y1} = \kappa(Z + z_0)u_* \frac{\partial \hat{v}_1}{\partial Z} + \sin\phi\left[2\alpha\hat{E}_1 - \frac{\kappa(Z + z_0)}{u_*}\hat{\varepsilon}_1\right]. \tag{18}$$

The following expressions have been used to derive (16)–(18):

$$E = E_0 + E_1, \qquad \varepsilon = \varepsilon_0 + \varepsilon_1, \qquad \alpha E_0 = u_*^2, \qquad \varepsilon_0 = \frac{u_*^3}{\kappa(Z + z_0)}. \tag{19}$$

The length scale $\kappa(Z + z_0)$ appears in the equation for ε_0 and elsewhere above as a consequence of the form assumed for the upstream profile, (7). For computations of flow above a surface with nonuniform surface roughness, $z_{01}(x, y)$, we shall adopt a similar procedure to that described in Section 2.2 for the simpler mixing-length closure. This will involve the use of a wall layer of depth Z_w such that, for $Z < Z_w$, specified forms of the variation of u_1, v_1, E_1, and ε_1 with Z will be assumed, while for $Z > Z_w$, the closure equations will be applied (see Section 2.4).

We shall expect ε to vary as $1/(Z + z_{01})$ near the surface. For uniform surface-roughness flows with $z_{01} \equiv z_0$, constant, this will lead to both ε_0 and ε_1 varying as $1/(Z + z_0)$ and, to avoid the 'near-singular' behaviour as $Z \to 0$, it is best to rewrite (17) as an equation for $\kappa(Z + z_0)\varepsilon_1$ and solve for this dependent variable in preference to ε_1. We shall, in fact, do this even for cases with nonuniform surface roughness but, with the conceptual use of a wall layer, the use of z_0 rather than z_{01} will be acceptable for $Z \geq Z_w \gg z_0, z_{01}$ only.

2.4. Boundary conditions

The surface boundary condition for velocity is expressed in the logarithmic profile which is assumed to be valid in a shallow 'wall' layer near the surface. This wall layer, of depth Z_w, must be shallow in comparison with the height, δ_I, to which the flow perturbations extend. It must also be greater than z_0 and z_{01} in order that the approximation, $Z + z_0 \simeq Z + z_{01}$ will be valid. The requirement that $\delta_I \gg Z_w \gg z_0, z_{01}$ will clearly lead to some constraints on the flow situations which can be studied with the model. We should remark that, for the linearized treatment of flows above variations in surface roughness, it is essential to make use of the wall-layer concept to get beyond the near-surface region within which $u_1 \simeq u_0$ and linearization will be invalid. Linearization will be valid for $Z \gg z_0, z_{01}$ provided the roughness change is not too great. The roughness changes are specified with respect to the reference or upstream roughness length z_0 by means of m_1 which is a function of X and Y. The actual roughness distribution relates to m_1 through:

$$z_{01}(X, Y) = z_0 e^{-m_1(X, Y)}. \tag{20}$$

Within the wall layer, the logarithmic velocity profile corresponding to a constant-

stress layer will be of the form:

$$u = u_0 + u_1 = \frac{\tau_x}{\kappa(\tau_x^2 + \tau_y^2)^{1/4}} \ln((Z + z_{01})/z_{01}),$$
$$v = v_0 + v_1 = \frac{\tau_y}{\kappa(\tau_x^2 + \tau_y^2)^{1/4}} \ln((Z + z_{01})/z_{01}). \tag{21}$$

This provides a relationship between velocity and stress which can be used as the lower boundary condition for the solution of the linearized equations for $Z > Z_w$. Provided $Z_w \gg z_0$, z_{01}, the logarithmic terms in (21) can be approximated by $\ln((Z + z_0)/z_0) + m_1$. Then, after linearization and transformation to Fourier space, we obtain:

$$\hat{u}_1 = \left[\frac{\hat{\tau}_{x1}}{\kappa u_*} - \frac{\cos\phi}{2\kappa u_*}(\hat{\tau}_{x1}\cos\phi + \hat{\tau}_{y1}\sin\phi)\right] \ln\frac{Z + z_0}{z_0} + \frac{u_*\cos\phi}{\kappa}\hat{m}_1,$$
$$\hat{v}_1 = \left[\frac{\hat{\tau}_{y1}}{\kappa u_*} - \frac{\sin\phi}{2\kappa u_*}(\hat{\tau}_{x1}\cos\phi + \hat{\tau}_{y1}\sin\phi)\right] \ln\frac{Z + z_0}{z_0} + \frac{u_*\sin\phi}{\kappa}\hat{m}_1. \tag{22}$$

We also assume that u is parallel to the surface throughout the wall layer and, for E – ε closure, that:

$$\frac{\partial E_1}{\partial Z} = 0, \qquad \frac{\partial(Z + z_{01})\varepsilon_1}{\partial Z} = 0.$$

After linearization and Fourier transformation, these give:

$$\hat{w}_1 = 0, \tag{23}$$

$$\frac{\partial \hat{E}_1}{\partial Z} = 0, \qquad \frac{\partial(Z + z_0)\hat{\varepsilon}_1}{\partial Z} = 0. \tag{24}$$

The use of z_0, rather than z_{01}, in (24) is only possible for $Z \gg z_0$. Furthermore, all of these lower boundary conditions should, in theory, be applied at $Z = Z_w \gg z_0$.

In practice, we adopt a different strategy. Notwithstanding all that we have said about the necessity to use a wall layer, we have, in fact, solved the governing sets of equations, (6) and either (9) or (16)–(18), right down to $Z = 0$, ignoring any changes in z_0 within the equations. As lower boundary conditions, we apply (22), (23) and, if appropriate, (24) at $Z = 0$. The solutions we obtain are invalid close to the surface but are valid for $Z \gg z_0$ and can be shown to be approximately equivalent to the solutions that would be obtained by using the wall-layer approach. The advantages of this seemingly devious procedure are that (a) the computer code is more readily vectorized, (b) we do not have to specify a particular depth for the wall layer nor carry out trial-and-error computations to determine its optimum depth, and (c) we can treat the topography- and roughness-induced flow perturbations in similar ways. Walmsley *et al.* (1986) adopted a somewhat

similar strategy in their MS3DJH/3R model. Conceptually one can regard the present approach as representing the effect of a roughness change as a slip velocity (positive or negative) at $Z = 0$.

The upper boundary conditions, after linearization and Fourier transformation are:

$$\hat{\tau}_{x1} = 0\,, \qquad \hat{\tau}_{y1} = 0\,, \qquad \hat{p}_1 = 0 \quad \text{for} \quad Z \to \infty \tag{25a}$$

and, for $E - \varepsilon$ closure:

$$\hat{E}_1 = 0\,, \qquad \hat{\varepsilon}_1 = 0 \quad \text{for} \quad Z \to \infty\,. \tag{25b}$$

2.5. Numerical method

Equations (6) and (9) or (16)–(18) form a closed set of ordinary differential equations subject to the boundary conditions described in Section 2.4. These equations have to be solved for all wavenumber pairs (k, m). For a high-resolution calculation with, for example, 256 × 256 gridpoints in the horizontal plane, we have to solve for 129 × 256 wavenumber pairs. To arrive at acceptable processing times, it was necessary to pay considerable attention to the efficiency of the code. Since we are working on a vector machine (CRAY-1S), it was necessary to ensure that most of the time-consuming parts of the code vectorized properly.

To minimize the number of vertical gridpoints necessary for acceptable accuracy, the gridpoints have to be distributed over the computational domain in a nonuniform way: more grid points in the regions with strong gradients and fewer gridpoints in the regions where the solution does not change very much. To accomplish this, we used knowledge about the behaviour of the solution. We know that the layer perturbed by topography can be divided into a shallow layer near the surface where turbulent stresses are important and an outer layer where the flow is pressure driven. The magnitude of the inner-layer thickness, l_i, is given by Hunt and Simpson (1982) as:

$$(l_i/L) \ln (l_i/z_0) = 2\kappa^2\,, \tag{26}$$

where L is the horizontal scale of the perturbation (topography- or roughness-induced). It can be shown that L should be inversely proportional to the horizontal wavenumber in the flow direction:

$$L = |k \cos\phi + m \sin\phi|^{-1}\,. \tag{27}$$

The outer layer, where pressure effects dominate the solution, has a thickness l_0 proportional to the horizontal scale of the perturbation (Hunt and Simpson, 1982):

$$l_0 = (k^2 + m^2)^{-1/2}\,. \tag{28}$$

Knowing that the solution has a logarithmic behaviour near the surface, the following coordinate transformation is postulated:

$$\eta = \frac{\ln[(Z + z_0)/z_0]}{\ln[(l_i + z_0)/z_0]} + Z/l_0\,. \tag{29}$$

With this transformation and a uniform grid on the η-axis, we only need 20 gridpoints to solve the set of differential equations for about 1% accuracy in the surface-stress values. This wavenumber-dependent scaling is possible because of the separation of scales by the Fourier transformation. The small horizontal scales are resolved by a grid over a shallow layer near the surface, whereas the gridpoints for the big horizontal scales are spread over a much thicker layer. The separation of scales and the possibility of a transformation that accounts for the different scales are major advantages of working in Fourier space.

Another way of limiting the number of gridpoints and, therefore, computing time, is by applying an asymptotic solution for large η as the upper boundary condition for the numerical solution. In the Jackson and Hunt (1975) theory, the stress terms are neglected in the outer layer, and the zero-order flow is assumed to be irrotational. With constant advection velocity u_0, v_0, the solutions for pressure and vertical velocity, excluding the trivial case with $k = m = 0$, are:

$$\hat{p}_1 = C e^{-\alpha_k Z}, \qquad \hat{w}_1 = -i\left[u_{op}\hat{f}_1 + C\,\frac{\alpha_k}{u_{op}}\,e^{-\alpha_k Z}\right], \tag{30}$$

where

$$\alpha_k = (k^2 + m^2)^{1/2}$$

and

$$u_{op} = ku_0 + mv_0 .$$

Since the solution contains an undetermined constant C, the boundary condition is specified as a relation between $\hat{w}_1$ and $\hat{p}_1$:

$$\hat{p}_1 = \frac{iu_{op}}{\alpha_k}\,\hat{w}_1 - \frac{u_{op}^2}{\alpha_k}\,\hat{f}_1 . \tag{31}$$

$\hat{u}_1$ and $\hat{v}_1$ can be expressed in terms of $\hat{p}_1$ by means of the inviscid equations and $\hat{\tau}_{x1}$ and $\hat{\tau}_{y1}$ can be evaluated by means of the closure assumption and $\hat{u}_1$ and $\hat{v}_1$. The latter is straightforward for the mixing-length approximation. In the $E - \varepsilon$ formulation it can be shown, by order of magnitude analysis, that $\hat{E}_1$ and $\hat{\varepsilon}_1$ can be neglected for $Z \gg l_i$. Therefore, $\hat{E}_1$ and $\hat{\varepsilon}_1$ are taken to be zero at the height where the boundary condition is applied. The advection velocity in the asymptotic solution is taken at the same height. Numerical experiments with the boundary conditions at different levels, η_B, showed that the solution becomes almost independent of η_B for $\eta_B > 3$ for all wavenumbers of practical interest ($10^3 < 2\pi/kz_0 < 10^7$).

In the $E - \varepsilon$ version, the outer length scale l_0 in (29) has been replaced by $10l_i$ in order to reduce the computational domain. The boundary has been applied at $\eta_B = 2.5$ in this version without significant loss of accuracy. This implies that the inviscid solution can be successfully applied in most of the outer layer.

The numerical method applied to solve the set of ordinary differential equations is a shooting technique. The equations are integrated from $\eta = 0$ to η_B with the known

boundary conditions specified at $\eta = 0$ and quite arbitrary values for the unknown variables. Independent solutions are calculated by integrating with different starting values at $\eta = 0$. One particular solution is computed for the roughness as well as the topographic case by choosing $\hat{m}_1 = 1$ and $\hat{f}_1 = 1$, respectively. The boundary conditions at $\eta = \eta_B$ are satisfied by solving linear equations for the coefficients of the independent solutions. The final solution is the sum of the particular solution and the independent solution multiplied by the appropriate coefficients.

A central differencing scheme is used for integration on a staggered, uniformly-spaced grid. Vectorization of the code is enhanced by treating a row of wavenumbers at the same time. This means that at many places in the code, a loop over all k-wavenumbers appears as an inner loop. The numerical integration of the equations for a run with

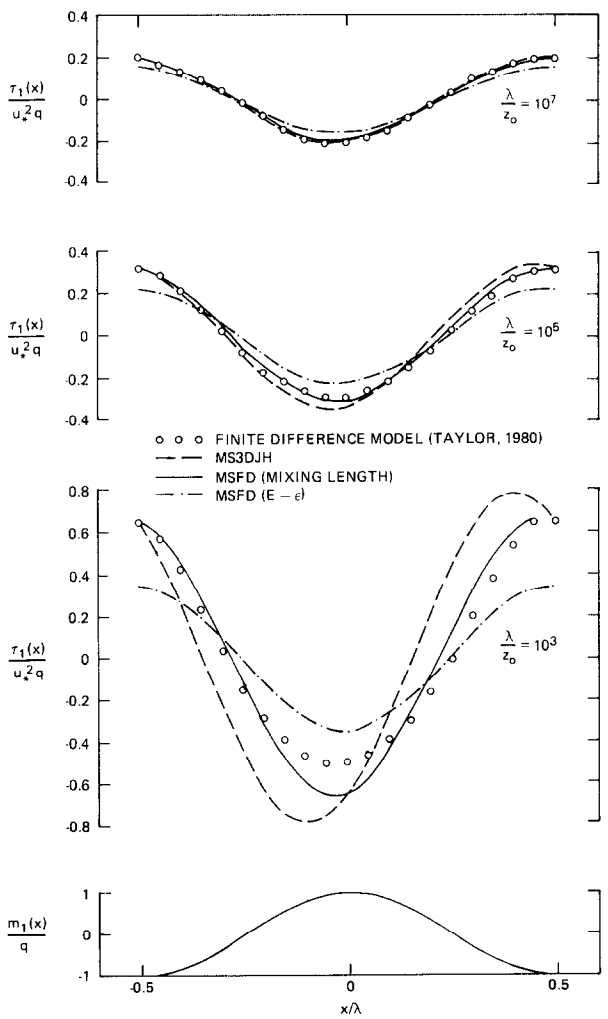

Fig. 1. Comparison of surface shear stress as calculated by four models for the sinusoidal roughness perturbation.

256 × 256 gridpoints in the horizontal plane and 20 in the vertical takes about 30 s with mixing-length closure and about 50 s with $E - \varepsilon$ closure on a CRAY-1S computer. The memory requirement is only about 200 K words since only one row of wavenumbers is in core at the same time.

3. Results for Roughness Perturbations

The simplest problem, in the context of the present model, is the situation where the logarithm of the surface roughness shows a small harmonic perturbation. For this case, we need one wavenumber only and assume:

$$m_1 = q \cos(2\pi x/\lambda), \tag{32}$$

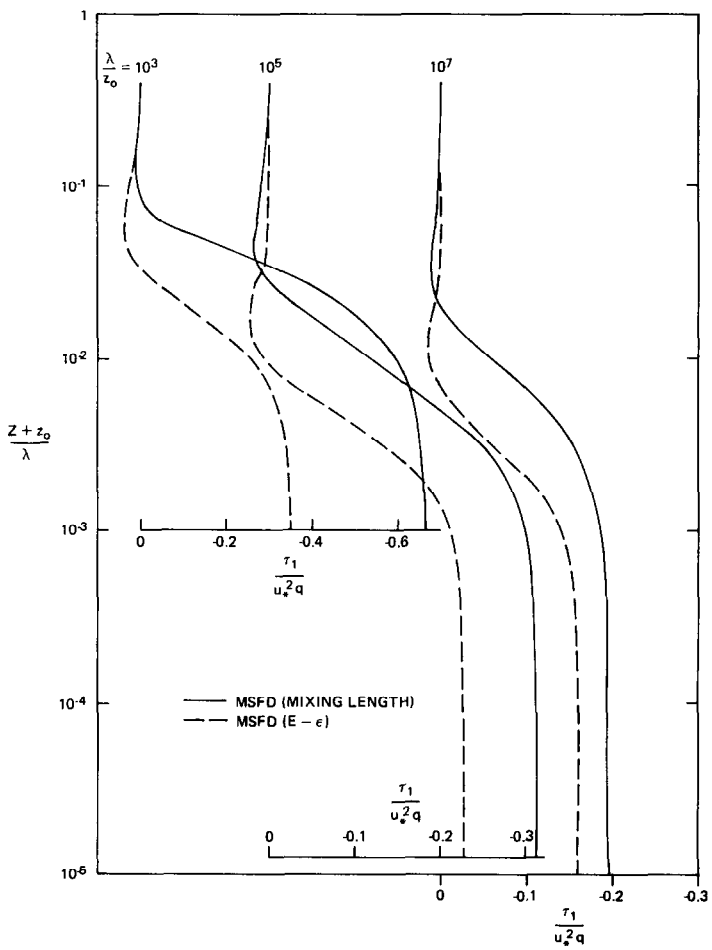

Fig. 2. Shear-stress profiles above the roughness minimum of a periodic sinusoidal roughness perturbation. MSFD has been applied with two closures.

where q is a small amplitude and λ is the wavelength of the perturbation. Note that a maximum in m_1 corresponds to a minimum in roughness length (see Equation (20)). The computations for the surface stress are shown in Figure 1 and compared with results from finite-difference calculations by Taylor (1978, 1980) and results from MS3DJH by Walmsley *et al.* (1986). The finite-difference calculations are based on a closure which is intermediate in complexity between the present mixing-length and $E - \varepsilon$ schemes. MS3DJH uses mixing-length closure and a constant advection velocity to arrive at analytic solutions. Calculations have been made for values of λ/z_0 in the range from 10^3 to 10^7, which covers most practical applications. Results for $\lambda/z_0 = 10^3$, 10^5, and 10^7 are shown in Figures 1–4. The profiles in Figures 2–4 are above the roughness minima (at $x = 0$). Values above the roughness maxima are equal in amplitude but opposite in sign. It is clear from Figure 1 that surface stresses from the present calculations with

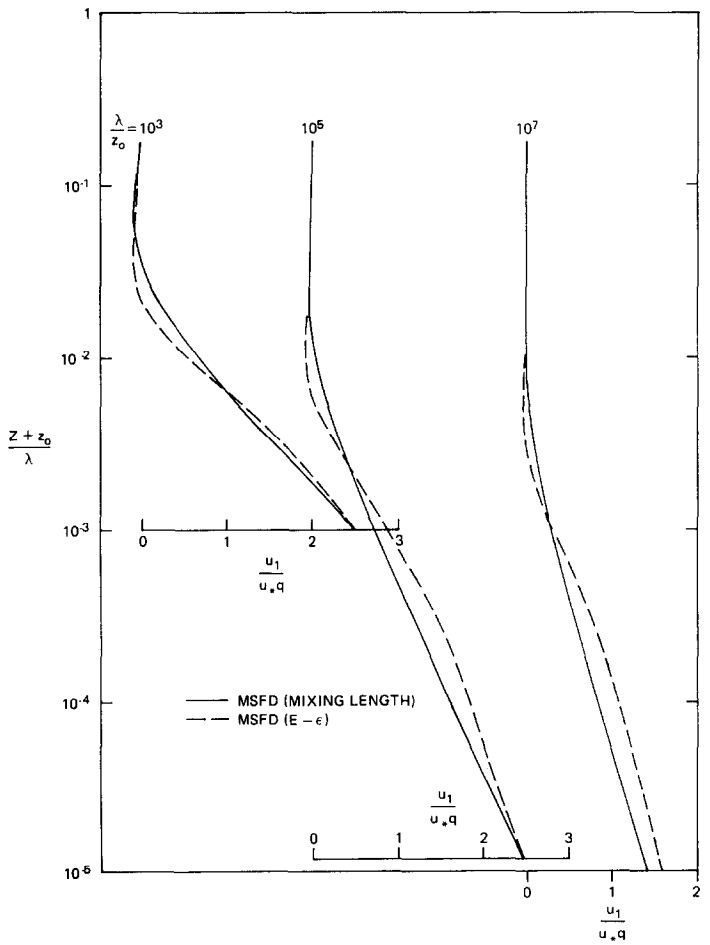

Fig. 3. Profiles of the MSFD velocity perturbation above the roughness minimum for the sinusoidal roughness boundary condition.

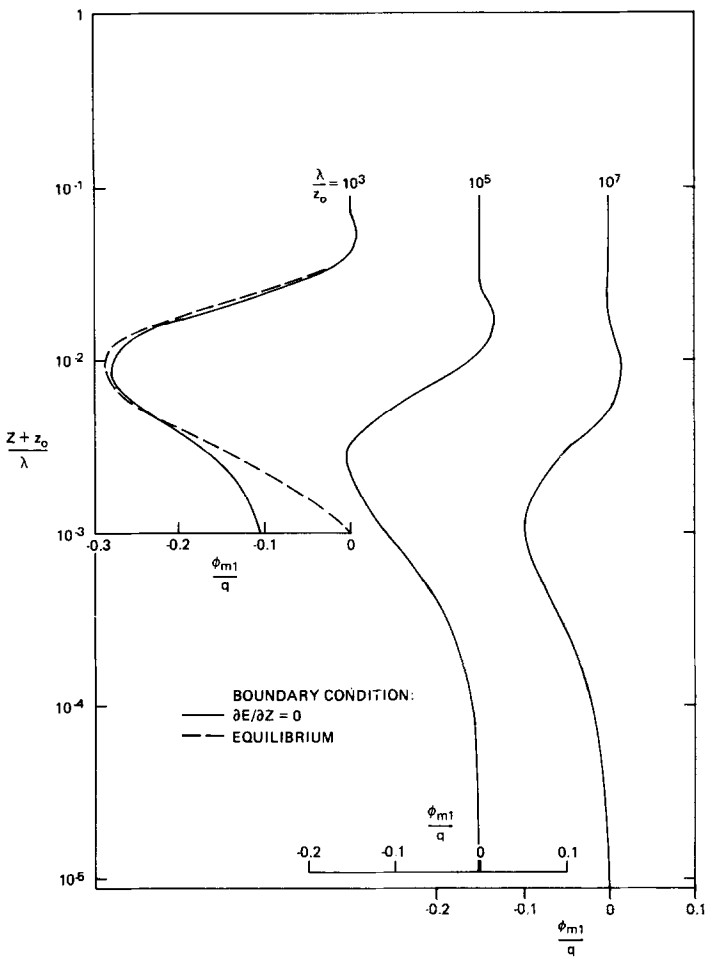

Fig. 4. Profiles of the MSFD ($E - \varepsilon$ closure) dimensionless wind-shear perturbation above the roughness minimum for the sinusoidal roughness boundary condition.

mixing-length closure compare better with finite-difference results than does MS3DJH. In particular, the phases of the surface-stress perturbation show good agreement in the present study. This is due to the full representation of the advection velocity as a function of height.

A significant result, shown by the present calculations, is the difference in surface stress and stress profiles between mixing-length and $E - \varepsilon$ closure model predictions. The latter predicts much smaller stress perturbations, particularly for small values of λ/z_0 and they are confined to a much shallower layer than is predicted by the mixing-length version of MSFD (see Figure 2 and Table I). Although the differences decrease for large values of λ/z_0, at $\lambda/z_0 = 10^7$ there is still a significant difference in stress predictions between the two closure schemes. In contrast to the stress results, we see relatively little difference in the velocity calculations between the two closures (see

TABLE I

Surface shear stress τ_1/qu_*^2 for the sinusoidal surface-roughness perturbation, Equation (32). The real part indicates the perturbation at $x = 0$; phase > 0 represents a shift in the positive x-direction.

λ/z_0	Mixing-length closure		$E - \varepsilon$ closure $\partial E/\partial Z = 0$ boundary condition		$E - \varepsilon$ closure equilibrium boundary condition	
	real part	phase (°)	real part	phase (°)	real part	phase (°)
10^3	−0.662	−12.3	−0.345	−1.9	−0.371	−6.0
10^4	−0.428	−10.8	−0.276	−4.0	−0.279	−5.1
10^5	−0.311	−9.6	−0.226	−5.7	−0.226	−5.9
10^6	−0.240	−8.4	−0.188	−6.0	−0.188	−6.0
10^7	−0.194	−7.2	−0.159	−5.7	−0.159	−5.7

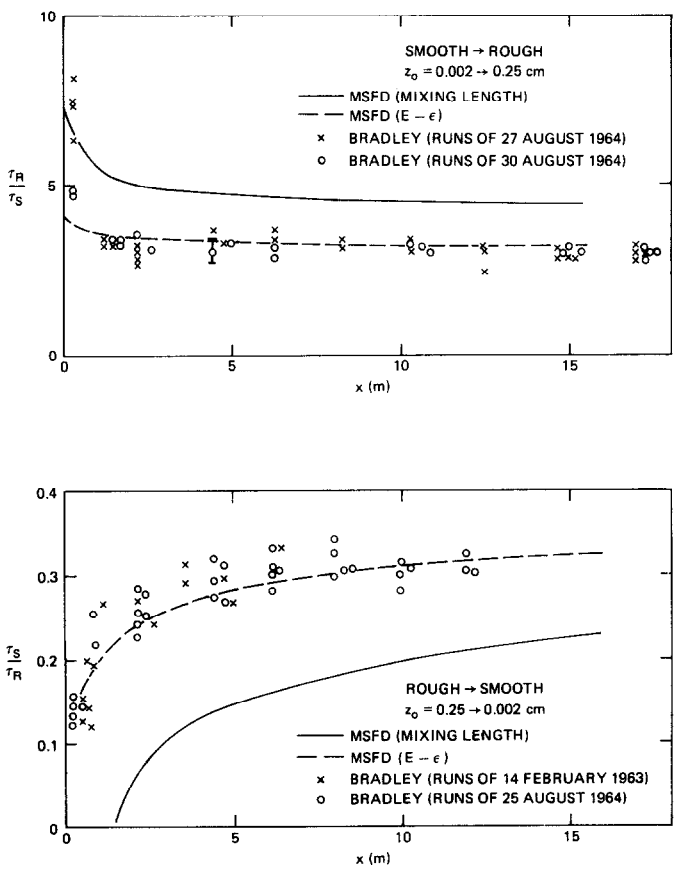

Fig. 5. Ratio of shear stresses as a function of distance from a step-change in roughness. MSFD compared with Bradley's (1968) data.

Figure 3). This is in agreement with the conclusions of a number of studies: velocity predictions are rather insensitive to the closure scheme.

An interesting parameter in the $E - \varepsilon$ model is the dimensionless shear:

$$\phi_m = \frac{\kappa(Z + z_0)}{\tau_x^{1/2}} \frac{\partial u}{\partial Z}, \quad \text{when} \quad v = \tau_y = 0. \tag{33}$$

The perturbation in ϕ_m for mean wind in the x-direction can be shown to be given by:

$$\phi_{m1} = \frac{\kappa(Z + z_0)}{u_*^3} \varepsilon_1 + \frac{1}{2} \frac{\tau_{x1}}{u_*^2} - 2 \frac{\alpha E_1}{u_*^2}, \qquad \text{for} \quad Z \gg z_0, \tag{34}$$

where the unperturbed value, $\phi_{m0} = 1$ for neutral flow. Figure 4 shows results for ϕ_{m1}. The minimum in ϕ_{m1} occurs roughly at the height where the stress gradient is large (at distances from the surface of the order l_i) but the nonzero ϕ_{m1} regime extends considerably below this and covers even a part of the layer where the stress is constant. This implies that, within the model, a constant-stress layer is not necessarily an equilibrium layer. It also implies that in cases where the horizontal scale is not very big compared to z_0 (for instance $\lambda/z_0 = 10^3$), there may not be a fully adapted layer near

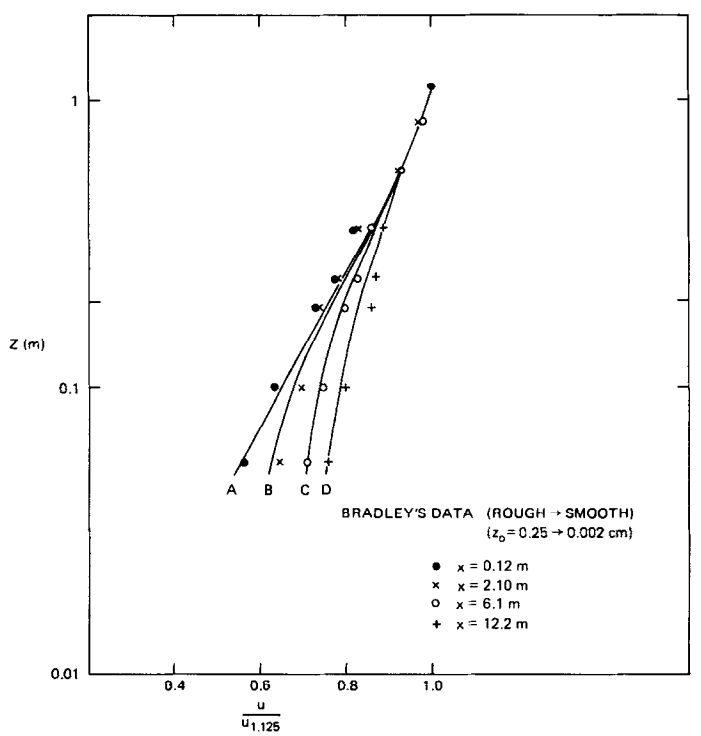

Fig. 6. Velocity profiles at different distances downstream of the rough-to-smooth transition. The MSFD model predictions with $E - \varepsilon$ closure (curves A, B, C, D) are compared with Bradley's (1968) data. Velocities have been normalized by the velocity at $Z = 1.125$ m.

the surface. In this case, ϕ_{m1} is different from zero even at the surface. The method of specifying the boundary conditions for $Z = 0$ then becomes questionable, but the alternative would be to calculate the flow around the individual roughness elements, which is a truly intractable problem. Figure 4 also shows the ϕ_{m1} profile for $\lambda/z_0 = 10^3$ when equilibrium is assumed to specify the boundary condition for $\hat{E}_1$ and $\hat{\varepsilon}_1$. The results are slightly different in a shallow layer near the surface. It is felt, however, that the assumption of zero-energy diffusion at the surface is physically more realistic.

Probably the most widely discussed surface-roughness modulation is the step-in-roughness problem and the most widely used atmospheric data set comes from Bradley's (1968) experiment. Although the present model cannot do the pure step-in-roughness problem because of the periodic boundary condition, it can simulate it as long as the internal boundary layer stays inside the adapted layer of the upstream transition.

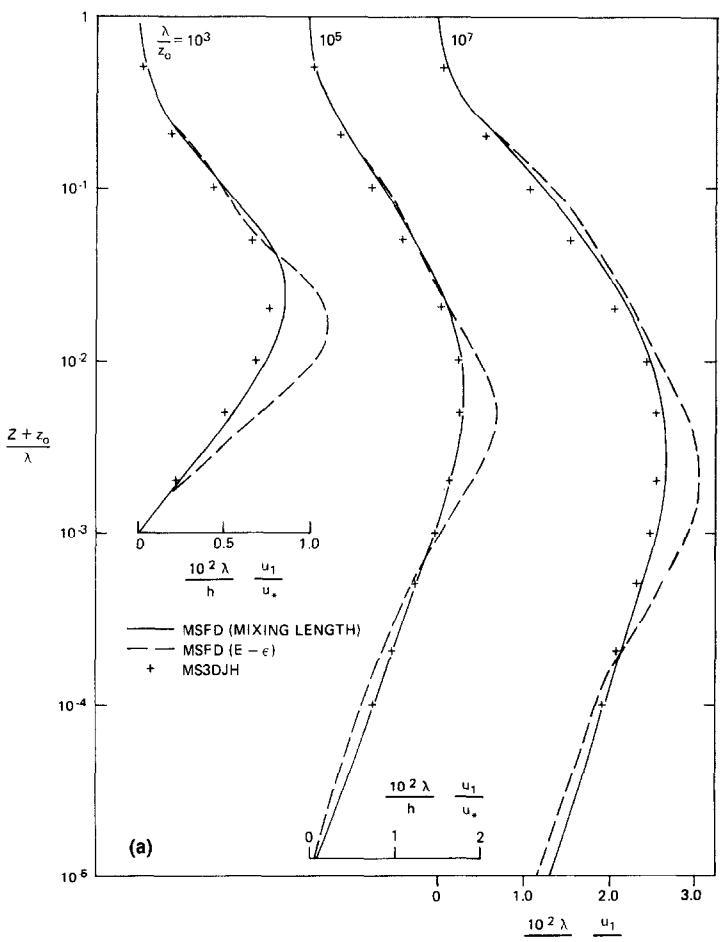

Fig. 7. Flow over sinusoidal topography of amplitude h. Profiles at the top of the hill ($x = 0$). (a) Velocity perturbation: comparison with MS3DJH/3 (Taylor *et al.*, 1983). (b) Phase of the velocity perturbation. Phase > 0 represents a shift of the velocity wave in the positive x-direction.

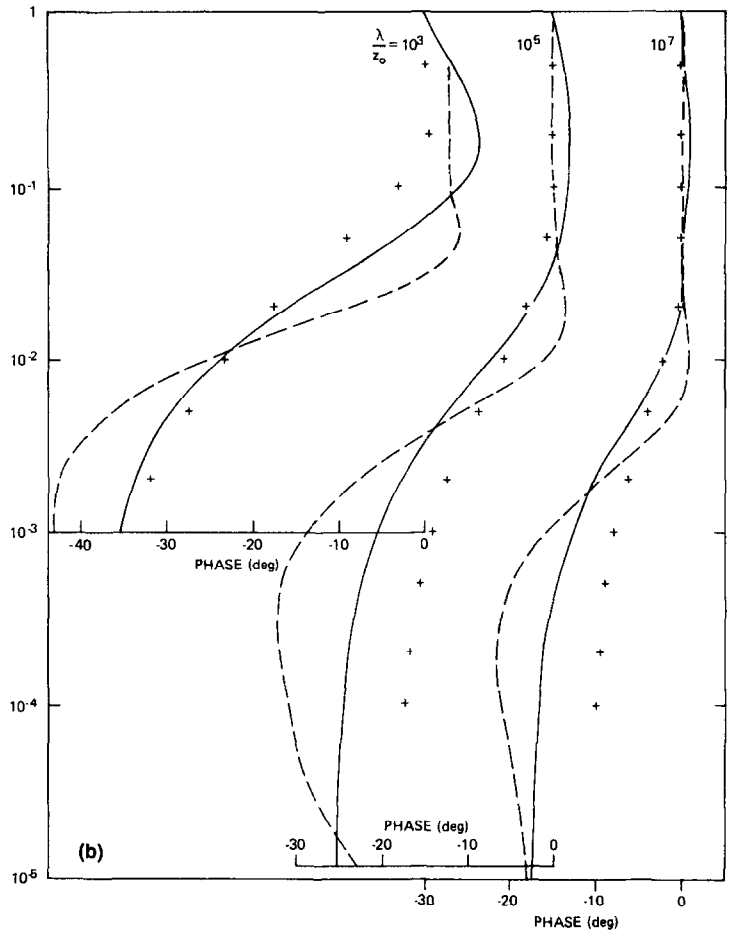

Here we shall consider a square-wave modulation in z_0 with $z_0 = 0.25$ cm for one-half of the cycle and $z_0 = 0.002$ cm for the other half. The results of the calculation just upstream of the transition are taken as the upstream condition for the step change and are subtracted from the results downstream of the step in order to find the perturbations due to the step change only. Walmsley *et al.* (1986) argue that the downstream roughness length should be taken as the reference value with respect to which perturbations should be calculated. They show that in this way the best correspondence is obtained between MS3DJH and numerical results from the nonlinear equations. Here a slightly different approach is followed. A linear theory obviously works best when the perturbations are small. With a given distribution of roughness, the perturbations are smallest when the reference state is taken as the average of maximum and minimum perturbation. The reference roughness length is thus taken as $z_0 = 0.022$ cm, which is the logarithmic average of 0.002 and 0.25 cm. As shown by Walmsley *et al.* (1986), the surface-stress calculations depend very little on the wavelength of the square-wave modulation. In principle, λ/z_0 should be chosen as large as possible, but we then lose resolution,

especially near the step change. To simulate Bradley's case, the length of the rough part was taken to be 22 m as in the experiment. The smooth part is also chosen as 22 m, making $\lambda = 44$ m.

Computations for the surface stress are compared with Bradley's data in Figure 5. The mixing-length closure overestimates the stress change; $E - \varepsilon$ closure gives much better results. Most simple closure schemes predict stress changes for this problem that are too large (see, for example, Shir, 1972, Figure 2). It should also be noted that quite a large uncertainty exists about the actual values of the roughness lengths in Bradley's experiment. The velocity profiles as predicted by MSFD with $E - \varepsilon$ closure are shown in Figure 6 for the rough-to-smooth transition. Results for the mixing-length closure are hardly different and are, therefore, not shown. The agreement with data is slightly better than with integral models (Townsend, 1966) and are comparable with Rao *et al.* (1974). Although the roughness change is quite big in Bradley's experiment, the linear approach predicts the surface stress and the wind profiles well. This suggests that the linear approximation will be sufficiently accurate in most practical situations. An exception might be the land-to-sea transition where the roughness ratio is of the order 10^3 whereas it is only of order 10^2 in Bradley's experiment.

4. Topographic Perturbations

We first consider, as a basic case, the topographic flow problem where the height of the surface is given by

$$f_1 = h \cos(2\pi x/\lambda), \tag{35}$$

where h is a small parameter. The velocity perturbation profiles at the top of the two-dimensional ridges are given in Figure 7a for model computations with both mixing-length and $E-\varepsilon$ closure. Figure 7b shows the phase profiles of the velocity perturbations. The MSFD model with mixing-length closure is equivalent to the Townsend (1972)

TABLE II

Surface pressure $p_1/10^2\,\rho u_*^2(h/\lambda)$ for the sinusoidal topographic perturbation, Equation (35). The real part indicates the perturbation at $x = 0$; phase > 0 represents a shift in the positive x-direction.

λ/z_0	Mixing-length closure		$E - \varepsilon$ closure		MS3DJH/3 Model[a]	
	real part	phase (°)	real part	phase (°)	real part	phase (°)
10^3	− 5.93	9.0	− 5.62	7.6	− 5.6	0.0
10^4	− 14.4	4.3	− 14.3	3.4	− 14.4	0.0
10^5	− 27.2	2.3	− 27.7	1.8	− 27.4	0.0
10^6	− 44.4	1.4	− 45.6	1.1	− 44.8	0.0
10^7	− 65.7	1.0	− 68.2	0.8	− 66.0	0.0

[a] Taylor *et al.* (1983). Note that h as defined there is double the value used in the present paper.

model for flow over small amplitude water waves. For testing purposes, the results of the MSFD code have been compared with Stubley's (see Taylor *et al.*, 1983) code for Townsend's model.

From Figure 7a, it is clear that the MS3DJH model (Taylor *et al.*, 1983) is very close to the mixing-length results as far as the velocity perturbation amplitudes are concerned. This is in spite of the rather crude representation of the advection profile in MS3DJH and omission of the perturbation vertical advection term. The phase profiles (Figures 7b), however, are more sensitive to the representation of the advection.

The results obtained with mixing-length and $E - \varepsilon$ closures are very similar for the surface pressure (see Table II) and agree with the MS3DJH/3 model (Taylor *et al.*, 1983). This supports the idea that the pressure is mainly determined by the inviscid equation and, therefore, independent of the closure formulation. This is also reflected in the velocity perturbations in the outer layer, the predictions of which are quite insensitive to the closure scheme. Closer to the surface, the predicted velocity perturbations are quite different with the extrema being more pronounced for the $E - \varepsilon$ closure (Figure 7a).

The main difference between results obtained with the two closure schemes is found in surface stresses (Table III) and the stress profiles (Figure 8). The $E - \varepsilon$ closure

TABLE III

Surface stress $\tau_1/10^2\, u_*^2 (h/\lambda)$ for the sinusoidal topographic perturbation, Equation (35). The real part indicates the perturbation at $x = 0$; phase > 0 represents a shift in the positive x-direction.

λ/z_0	Mixing-length closure		$E - \varepsilon$ closure	
	real part	phase (°)	real part	phase (°)
10^3	0.282	− 36.1	0.179	− 38.2
10^4	0.274	− 31.5	0.200	− 30.3
10^5	0.257	− 25.8	0.205	− 24.4
10^6	0.240	− 21.0	0.203	− 20.0
10^7	0.226	− 17.4	0.199	− 15.4

predicts smaller amplitudes for the stress perturbation, even for very large λ/z_0 ratios where the flow has a long distance to adapt to the new surface condition.

It is interesting to make a brief comment here on the consequences of $E - \varepsilon$ closure on similar problems that have been studied earlier. The use of $E - \varepsilon$ closure instead of simpler schemes for flow over water waves (Townsend, 1972) would hardly change the growth rates of the waves as computed by Townsend, since the wave instability is mainly pressure-driven and, therefore, not altered by the closure. However, the growth rates of sand ripples, as predicted by Richards (1980) will change with $E - \varepsilon$ closure since sediment transport is determined by the surface stress.

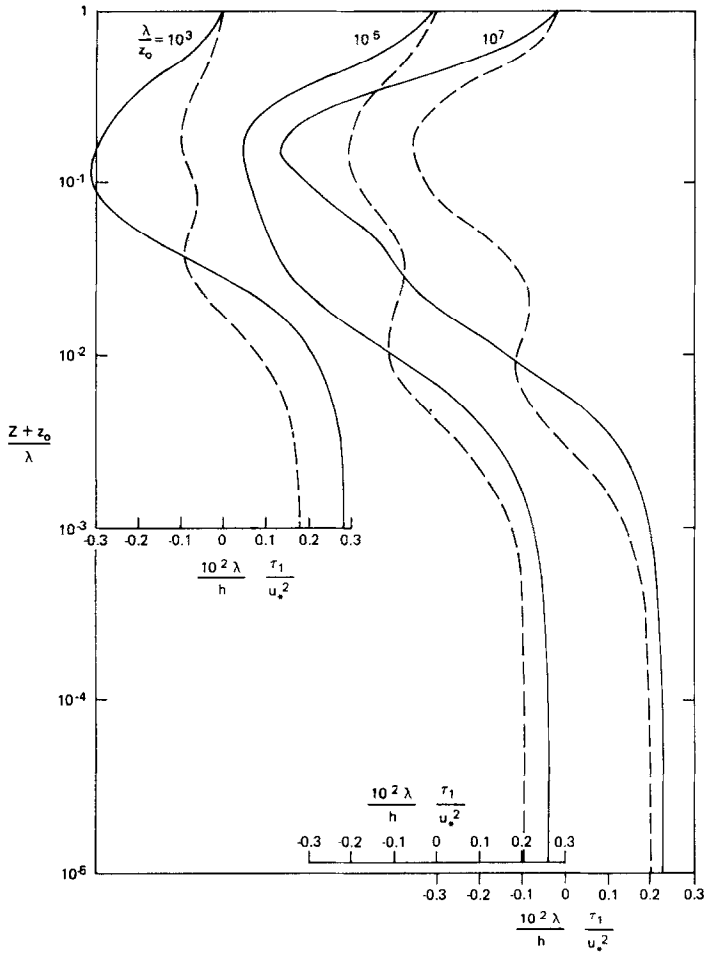

Fig. 8. Stress perturbation at $x = 0$ for flow over sinusoidal topography.

5. Application of the MSFD Model to Real Terrain: Askervein Hill

Askervein is an isolated hill located on the island of South Uist in the Outer Hebrides of Scotland. Its maximum height is 126 m above mean sea level while the surrounding terrain varies between about 8 and 12 m. The surface roughness is taken as $z_0 = 0.03$ m and uniform. A contour map of the height distribution is shown in Figure 9. There has been an extensive field program to investigate the mean flow and turbulence structure at different locations on the hill (see Taylor and Teunissen, 1985). Selected tower locations are indicated on Figure 9.

For computational purposes, the contour information has been transformed to gridpoint values. The grid consists of 256 × 256 points uniformly distributed over an area of 6400 × 6400 m. This makes the resolution 25 m and the domain sufficiently big to avoid upstream effects due to the periodic boundary conditions. Since many of the

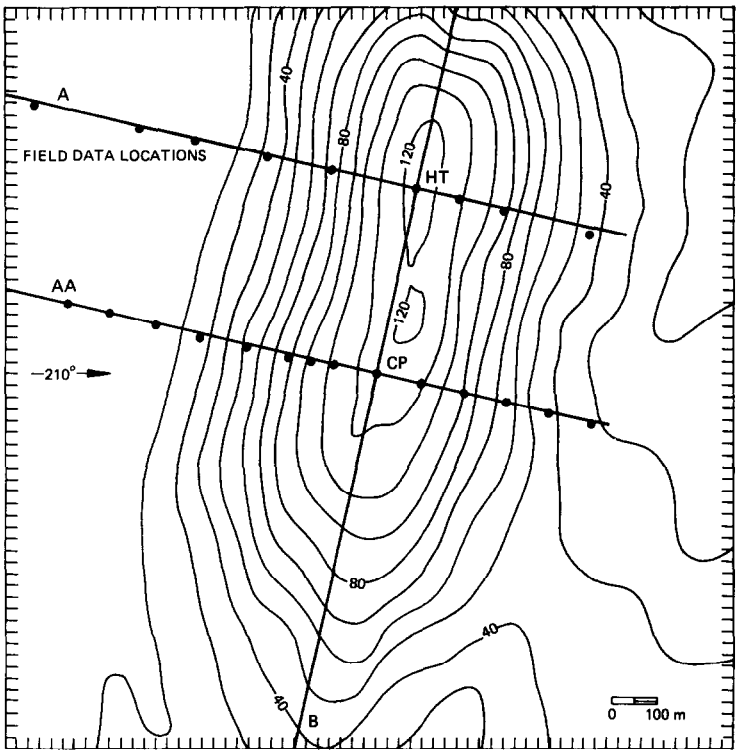

Fig. 9. Contour map of Askervein showing full-scale experiment tower lines and data positions plotted in Figures 10a and 10b. Contour interval is 10 m. Map is oriented so that 210° (the wind direction for the case shown in Figures 10–12) is towards the left. The orientation of the tower lines A and AA is 223°–043° and the B-line is perpendicular. MSFD grid spacing (25 m) is shown by tick marks on the perimeter. Area plotted is the central portion (64 × 64 grid points or 1575 × 1575 m) of a 256 × 256 gridpoint periodic domain (6400 × 6400 m).

experimental data were taken for wind directions close to 210°, all the model runs were done for this wind direction. This is only 13° from perpendicular to the orientation of the ridge.

Results are presented in Figure 10 in terms of the fractional speed-up ratio, ΔS. This is the ratio of the wind speed perturbation to the upstream speed, both at $Z = 10$ m. Figure 10a shows cross-sections along tower line AA. This is considered to be the centreline and crosses point CP, whereas Figure 10b shows cross-sections along the A tower line which crosses the hilltop (HT). The data are from Runs TU25, TU03-A and TU03-B of the 1983 Askervein experiment (Taylor and Teunissen, 1985; Walmsley and Salmon, 1984). Different models are compared: MSFD with mixing-length and $E - \varepsilon$ closures, MS3DJH/3 (Walmsley and Salmon, 1984) and an $E - \varepsilon$ finite-difference model by Raithby and Stubley (1985). From the latter, only a portion of the results in the wake region is shown since it is the only place where they are considerably different from the other models. Also plotted in Figure 10 are the topographic cross-sections, f_1, shown without vertical exaggeration, and the points CP and HT.

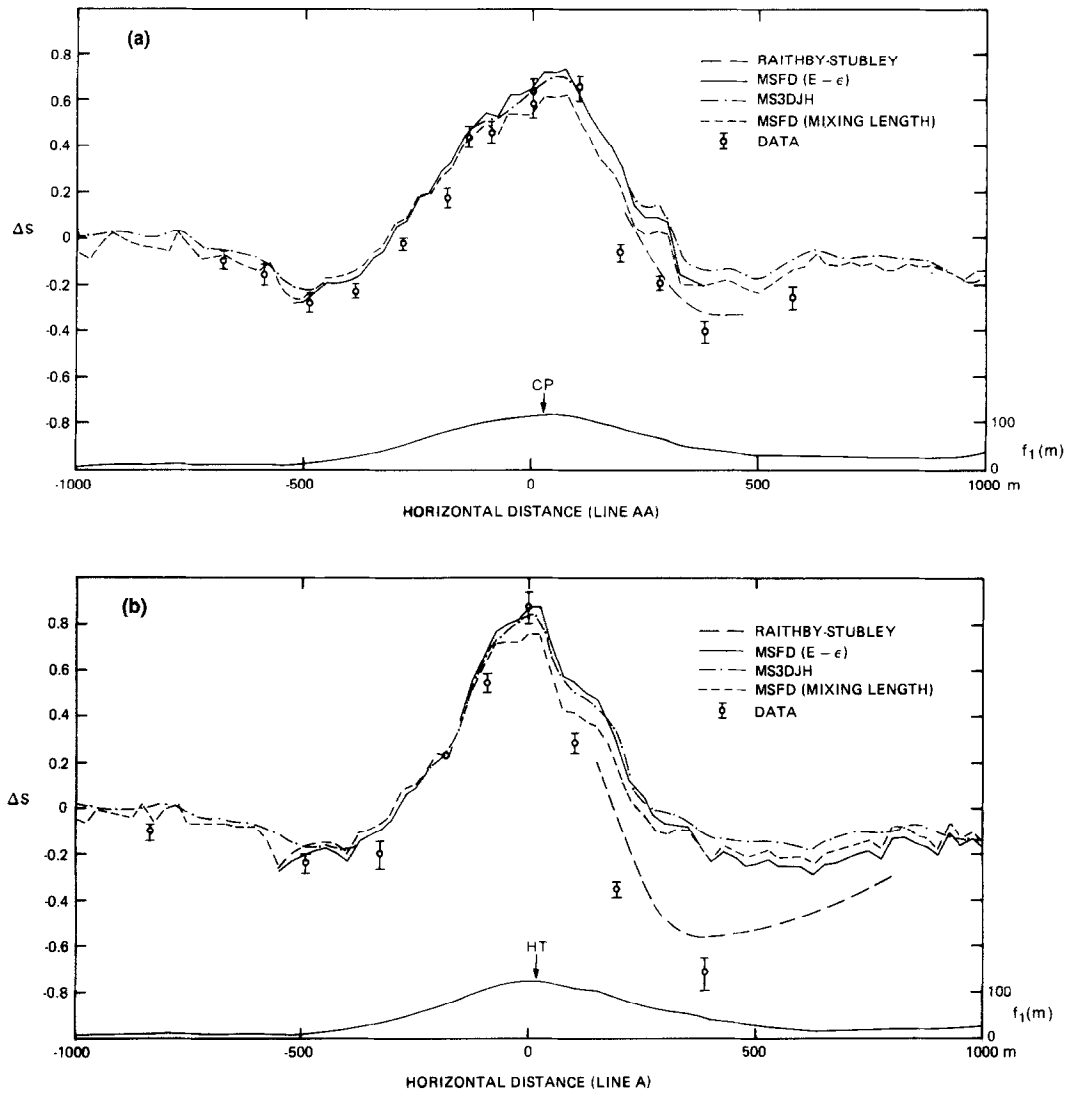

Fig. 10. Fractional speed-up ratios for flow over Askervein (see Figure 9) at a height of 10 m above terrain. Comparison of different model results and experimental data. Wind direction is 210°; roughness length is 0.03 m. Topographic cross-sections are also shown, without vertical exaggeration. (a) Cross-section along line AA. (b) Cross-section along line A.

In Figure 10a, the two MSFD curves and the MS3DJH/3 curve exhibit quite similar behaviour. The MS3DJH/3 grid is oriented along the wind direction and is thus not exactly along the tower lines, as was the case for MSFD. To obtain values along the AA and A lines requires interpolation which causes slightly smoother results. The three curves are in almost complete agreement on the upwind slope ($x < 0$). The two MSFD curves are essentially superimposed in the flat regions upstream and downstream of the Askervein hill. MSFD ($E - \varepsilon$) and MS3DJH/3 give almost identical results on the upper

part of the downwind slope ($x > 0$). Near the summit of the ridge ($x \sim 50$ m) the MSFD (mixing-length) model gives $\Delta S \sim 0.62$, whereas MS3DJH/3 gives $\Delta S \sim 0.70$ with MSFD ($E - \varepsilon$) quite close at ~ 0.72.

Looking now at smaller-scale features in the ΔS results, the various peaks and troughs can be related to small changes in slope of the terrain, scarcely noticeable on the topographic cross-section. The peak at $x = -925$ m, for example, is related to an increase in elevation of 4 m in $\Delta x = 50$ m, i.e., a slope of 0.08. The peak at $x = -775$ m occurs at a small ridge of height about 2 m and horizontal extent about 50 m. The trough at $x = -525$ m is related to a 2-m depression in the terrain along the cross-section. The trough at $x = -75$ m is due to a change in slope from ~ 0.07 to ~ 0.02 over $\Delta x \sim 75$ m. The local maximum at $x = 275$ m is also related to a change in slope, from -0.08 to -0.06 over $\Delta x \sim 50$ m. Finally, the small peak at $x = 625$ m can be traced to a small ridge of about 0.6 m height. The model flow, therefore is sensitive to small slope changes in what, at first glance, appears to be a rather smooth hill without small-scale features.

Agreement of the MSFD and MS3DJH/3 models with the data is excellent at the summit of the ridge and upwind ($x < 0$). The local minimum at $x = -75$ m is apparent in the data. MSFD ($E - \varepsilon$) and MS3DJH/3 seem to represent the flow at the summit of the ridge better than MSFD (mixing-length). The Raithby–Stubley model results agree much better with the data on the downwind slope, probably because of inclusion of nonlinear effects, but they fail to resolve the local feature at $x \sim 275$ m which also appears in the data. Elsewhere the Raithby–Stubley model results are similar to those of MSFD and MS3DJH/3 except that they do not show the small-scale features and they are obtained at much greater computing cost.

The above discussion on Figure 10a applies quite well to Figure 10b, the main exception being that all three curves are slightly different in the downwind flat region ($x > 0$). Due to the fact that HT is slightly higher than CP, the slopes are necessarily steeper and the maxima slightly larger. Values of ΔS reach ~ 0.76 for MSFD (mixing-length), ~ 0.84 for MS3DJH/3 and ~ 0.88 for MSFD ($E - \varepsilon$). Small-scale features in the ΔS cross-sections can again be related to local changes in terrain slope. Agreement of MSFD and MS3DJH/3 with the data is excellent at the summit and upwind ($x < 0$), with MSFD ($E - \varepsilon$) giving the best agreement at the summit itself. The Raithby–Stubley model performs significantly better on the downwind side ($x > 0$) and about the same elsewhere, although, again small-scale features are not apparent.

The main conclusion is that the differences between the models' predictions are quite small and that $E - \varepsilon$ does slightly better than the simpler closure schemes. An exception for this conclusion is the wake region where Raithby and Stubley (1985) have better results. Nonlinear effects may be important here, although the effect of a smaller hill downwind which was resolved by Raithby and Stubley, but not by MSFD, must also be considered. Wind speed profiles at the top of the hill are shown in Figure 11. Results from models using $E - \varepsilon$ closure show better agreement with the field data than do mixing-length models; in particular, the speed-up ratio near the surface is predicted better.

The main difference between the mixing-length closure and $E - \varepsilon$ closure shows up

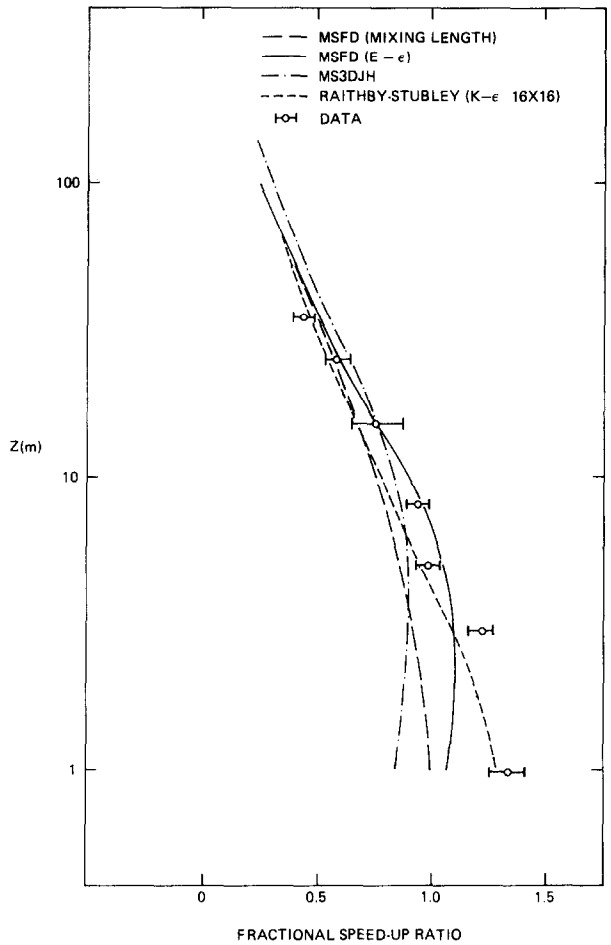

Fig. 11. Profile of fractional speed-up at the top (point HT) of Askervein hill. Comparison of different model results and experimental data. Same case as Figure 10a.

in the shear-stress predictions (see Figure 12); $E - \varepsilon$ predicts much smaller stress perturbations. Two regions have to be distinguished in Figure 12: (i) the inner layer where the problem is shear-dominated and (ii) the outer region where the flow is pressure-driven. It seems as if the predicted inner-layer thickness is too thick, which might be due to a wrong estimate of the surface roughness. Zeman and Jensen (1985) who did computations for the same hill with a more complex closure scheme had the same problem and suggested that the surface roughness at the top of the hill might be much smaller than 0.03 m. This additional roughness change would cause a negative surface-stress perturbation at the top of the hill and, therefore, move the zero-crossing point towards the surface. In the outer layer, there are big differences between the two closure schemes and with the data. In the inviscid region, there is a factor 2 difference

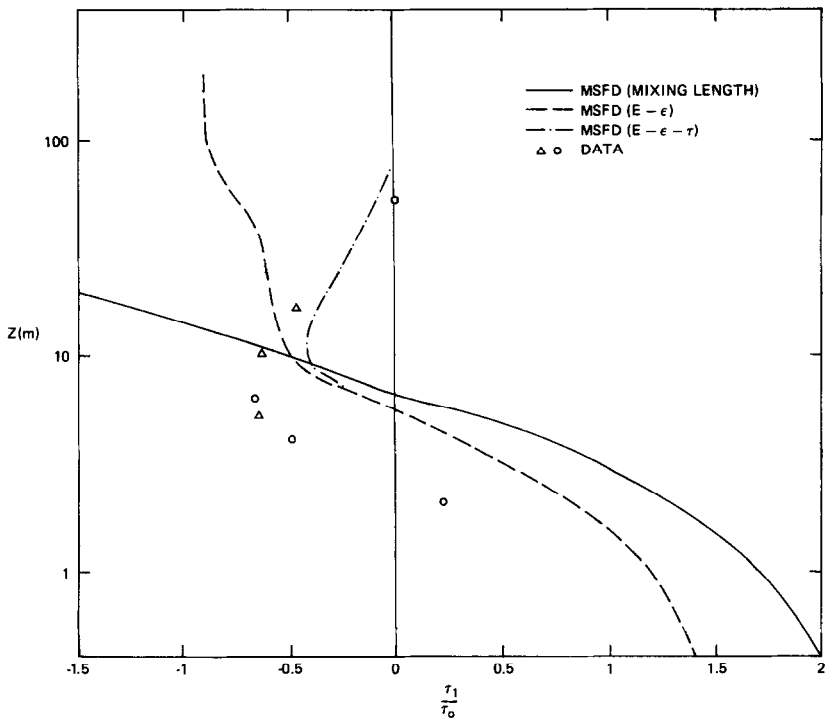

Fig. 12. Profile of dimensionless stress at the top (point HT) of Askervein hill. Model results compared with data. Same case as Figure 10a. Data from Zeman and Jensen (1985).

in the asymptotic expressions (9) and (18). Neither closure scheme seems to be very realistic. The mixing-length closure assumes that the stress and the exchange coefficient respond instantaneously to the changing shear; $E - \varepsilon$ closure also assumes in the outer layer that the stress responds instantaneously to the new shear, but with no change to the upstream value for the exchange coefficient. This accounts for the factor 2 difference. It seems more likely, however, that the shear stress responds only slowly to the shear, which implies that a differential equation would be needed for the shear stress itself. On the other hand, we are reasonably confident that the shear stress is well predicted near the surface with $E - \varepsilon$ closure.

To improve the stress-profile calculations, a simple equation (proposed by Launder, 1975) has been tried for the shear stress:

$$u \frac{\partial \tau_x}{\partial x} + v \frac{\partial \tau_x}{\partial y} + w \frac{\partial \tau_x}{\partial z} = -C_3 \left[\frac{\varepsilon}{E} \tau_x - \alpha^2 E \frac{\partial u}{\partial z} \right], \tag{36}$$

with a similar equation for τ_y. This equation originally had a diffusion term as well, which has been neglected here to simplify the computations. The diffusion effect in the shear stress is expected to be small in the outer layer where the shear is caused by the pressure gradient. Near the surface, the two terms at the right-hand side of (36) balance, implying

that the equation reduces to (10). The results in the outer layer are quite insensitive to the value of C_3 for which 1.5 is chosen as proposed by Launder (1975).

In linear form, the τ_{x1} and τ_{y1} equations read:

$$\hat{\tau}_{x1}\left[1 + \frac{\kappa(Z + z_0)}{C_3 u_*}\,(iku_0 + imv_0)\right] = \kappa(Z + z_0)u_* \frac{\partial \hat{u}_1}{\partial Z} + (\cos\phi)\left[2\alpha\hat{E}_1 - \frac{\kappa(Z + z_0)}{u_*}\,\hat{\varepsilon}_1\right], \tag{37}$$

$$\hat{\tau}_{y1}\left[1 + \frac{\kappa(Z + z_0)}{C_3 u_*}\,(iku_0 + imv_0)\right] = \kappa(Z + z_0)u_* \frac{\partial \hat{v}_1}{\partial Z} + (\sin\phi)\left[2\alpha\hat{E}_1 - \frac{\kappa(Z + z_0)}{u_*}\,\hat{\varepsilon}_1\right]. \tag{38}$$

From these equations it is quite clear that corrections to $E - \varepsilon$ closure (18) are only significant when $(Z + z_0)\,(ku_0 + mv_0)/u_* \; O(1)$, which occurs outside the inner layer. This implies that the extra equation for shear stress has no effect on the dynamics of the flow. It only changes the shear-stress results where the velocity and the velocity gradient are pressure-driven. This is also the reason that inclusion of (37) and (38) in the closure causes no significant change in the surface pressure and surface stress for the sinusoidal problems (Tables I, II, and III for $E - \varepsilon$ closure also apply for $E - \varepsilon - \tau$ closure).

The stress profile on top of Askervein hill, however, looks much more realistic with the $E - \varepsilon - \tau$ closure (see Figure 12). It still appears as if the profile does not have the appropriate scaling near the surface. The differences between model and data might be caused by roughness change (as noted earlier) or perhaps by streamline-curvature effects which are not accounted for in the present model but are known to have a considerable effect on the turbulence structure (see Zeman and Jensen, 1985).

6. Conclusion

A mixed spectral finite-difference (MSFD) model has been proposed for neutrally stratified surface-layer flow over complex terrain. The model predicts velocity perturbations and some turbulence characteristics for an arbitrary distribution of surface roughness and surface height. Although the theory is linear and assumes small perturbations, it produces satisfactory results for a roughness ratio of 100 and for hills with slopes of order 0.3. The linear approach has the advantage that (i) arbitrary surface boundary conditions are very simple to deal with, (ii) the computational method is very simple and accurate because of the wavenumber-dependent vertical scaling, and (iii) the computer requirements for memory and processing time are very limited even for high-resolution runs.

Two closure schemes have been investigated for roughness modulations, viz., mixing-length and $E - \varepsilon$. The difference between the two schemes is small as far as the velocity perturbations are concerned. The surface-stress perturbations, however, are smaller and compare better with data in the case of $E - \varepsilon$ closure. Also the deviation from equilibrium as shown by Peterson (1969a) and Beljaars *et al.* (1983) for flow over changing surface roughness, is more realistically represented with $E - \varepsilon$ closure.

Three closure schemes have been investigated for flow over low hills, viz., mixing-length, $E - \varepsilon$ and $E - \varepsilon - \tau$. The last of these has a simple advection equation for the shear stress. The conclusions for flow over low hills can be summarized as follows:

– The closure scheme has a negligible effect on the pressure perturbations. This suggests that an inviscid approximation would be sufficient to compute pressure as in the MS3DJH models. A real representation of the unperturbed advection profile would, however, probably be better than the irrotational-flow assumption in the Jackson and Hunt (1975) theory.

– The velocity perturbations in the outer layer are independent of the closure scheme since the flow is pressure-driven there.

– The speed-up in the inner layer near the top of a hill is larger with $E - \varepsilon$ closure than with mixing-length and compares better with experimental data. The inner-layer results are not changed when an equation for the shear stress is added.

– Shear-stress perturbations as predicted with mixing-length closure are too large in the inner layer and much too large in the outer layer.

– The $E - \varepsilon$ predictions for shear stress are acceptable in the inner layer but still too large in the outer layer. It is suggested that an advection equation for shear stress is needed here to replace the eddy diffusivity assumption which assumes instantaneous response to shear.

– The linear approximation seems to work quite well for Askervein hill (slope of the order 0.3) except in the lee of the hill where nonlinear effects may be present.

Acknowledgements

Most of the work presented in this paper was done during the first author's leave from KNMI, which is greatly acknowledged. We wish to thank Judy Selmes-Brymer for typing the manuscript, Brian Taylor and Kristina Czaja for drafting the figures, and Stephen Karpik for his comments.

References

Antonia, R. A. and Luxton, R. E.: 1971, 'The Response of a Turbulent Boundary Layer to a Step Change in Surface Roughness. Part 1. Smooth to Rough', *J. Fluid Mech.* **48**, 721–761.

Beljaars, A. C. M., Schotanus, P., and Nieuwstadt, F. T. M.: 1983, 'Surface Layer Similarity under Nonuniform Fetch Conditions', *J. Clim. Appl. Meteorol.* **22**, 1800–1810.

Bradley, E. F.: 1968, 'A Micrometeorological Study of Velocity Profiles and Surface Drag in the Region Modified by a Change in Surface Roughness', *Quart. J. Roy. Meteorol. Soc.* **94**, 361–379.

Caneill, J. Y., Buty, D., and Saab, A. E.: 1985, *Sensitivity Studies Related to Turbulence Parameterizations for*

Numerical Simulations of Mesoscale Flows over Complex Terrain, Seventh Symp. Turb. Diff., Amer. Meteorol. Soc., November 12–15, Boulder, Co.

Detering, H. W. and Etling, D.: 1985, 'Application of the $E - \varepsilon$ Turbulence Closure Model to the Atmospheric Boundary Layer', *Boundary-Layer Meteorol.* **33**, 113–133.

Durst, F., Launder, B. E., Schmidt, F. W., and Whitelaw, J. H.: 1979, *Turbulent Shear Flows I*, Springer-Verlag, Berlin, 415 pp.

Hunt, J. C. R. and Simpson, J. E.: 1982, 'Atmospheric Boundary Layers over Non-Homogeneous Terrain', in E. J. Plate (ed.), *Engineering Meteorology*, Elsevier, Amsterdam.

Jackson, N. A.: 1976, 'The Propagation of Modified Flow Downstream of a Change in Roughness', *Quart. J. Roy. Meteorol. Soc.* **102**, 924–933.

Jackson, P. S. and Hunt, J. C. R.: 1975, 'Turbulent Wind Flow over a Low Hill', *Quart. J. Roy. Meteorol. Soc.* **101**, 929–955.

Launder, B. E.: 1975, *Progress in the Modelling of Turbulent Transport*, Lecture notes presented at the von Kármán Institute, Rhode-St.-Genese, Belgium, March 3–7.

Lumley, J. L. and Khajeh-Nouri, B.: 1974, 'Computational Modelling of Turbulent Transport', *Adv. Geophys.* **18A**, 169–192.

Mason, P. J. and Sykes, R. I.: 1979, 'Flow over an Isolated Hill of Moderate Slope', *Quart. J. Roy. Meteorol. Soc.* **105**, 383–395.

Mellor, G. L. and Yamada, T.: 1974, 'A Hierarchy of Turbulence Closure Models for Planetary Boundary Layers', *J. Atmos. Sci.* **31**, 1791–1806.

Mellor, G. L. and Yamada, T.: 1982, 'Development of a Turbulence Closure Model for Geophysical Fluid Problems', *Rev. Geophys. Space Phys.* **20**, 851–875.

Nieuwstadt, F. T. M. and Van Dop, H. (eds.): 1982, *Atmospheric Turbulence and Air Pollution Modelling*, D. Reidel Publ. Co., Dordrecht, Holland.

Panofsky, H. A. and Dutton, J. A.: 1984, *Atmospheric Turbulence: Models and Methods for Engineering Applications*, John Wiley and Sons, New York.

Panofsky, H. A. and Townsend, A. A.: 1964, 'Change of Terrain Roughness and the Wind Profile', *Quart. J. Roy. Meteorol. Soc.* **90**, 147–155.

Peterson, E. W.: 1969a, 'On the Relation Between the Shear Stress and the Velocity Profile After a Change in Surface Roughness', *J. Atmos. Sci.* **26**, 773–774.

Peterson, E. W.: 1969b, 'Modification of Mean Flow and Turbulent Energy by Change in Roughness Under Conditions of Neutral Stability', *Quart. J. Roy. Meteorol. Soc.* **95**, 561–575.

Raithby, G. D. and Stubley, G. D.: 1985, *Prediction and Comparison with Experiment of Three-Dimensional Flow over the Askervein Hill*, Rep. Thermal Science Ltd., Waterloo, Ont., Canada.

Rao, K. S., Wyngaard, J. C., and Coté, O. R.: 1974, 'The Structure of the Two-Dimensional Internal Boundary Layer over a Sudden Change of Surface Roughness', *J. Atmos. Sci.* **31**, 738–746.

Richards, K. J.: 1980, 'The Formation of Ripples and Dunes on an Erodible Bed', *J. Fluid Mech.* **99**, 597–618.

Rodi, W.: 1980, *Turbulence Models and Their Applications in Hydraulics: A State-of-the-Art Review*, Inst. für Hydromechanik, Univ. of Karlsruhe, Germany.

Shir, C. C.: 1972, 'A Numerical Computation of Air Flow over a Sudden Change of Surface Roughness', *J. Atmos. Sci.* **29**, 304–310.

Taylor, P. A.: 1969, 'On Wind and Shear Stress Profiles Above a Change in Surface Roughness', *Quart. J. Roy. Meteorol. Soc.* **95**, 77–91.

Taylor, P. A.: 1978, *A Note on Velocity and Turbulent Energy Profiles in the Surface Layer with Particular Reference to the Numerical Modelling of Turbulent Boundary-Layer Flow Above Horizontally Inhomogeneous Terrain*, Internal Rep. ARQL 4/78, Atmos. Environ. Service, Downsview, Ont., Canada, 36 pp.

Taylor, P. A.: 1980, 'Some Recent Results from a Numerical Model of Surface Boundary-Layer Flow over Hills', in J. C. Wyngaard (ed.), *Workshop on the Planetary Boundary Layer*, Amer. Meteorol. Soc., Boston, pp. 150–157.

Taylor, P. A. and Teunissen, H. W.: 1985, *The Askervein Hill Project: Report on the September/October 1983 Main Field Experiment*, Internal Rep. MSRB-84-6, Atmos. Environ. Service, Downsview, Ont., Canada.

Taylor, P. A., Mason, P. J., and Bradley, E. F.: 1985, *Boundary Layer Flow over Low Hills – A Review of Recent Field Experiments*, Seventh Symp. Turb. Diff., Amer. Meteorol. Soc., November 12–15, Boulder, Co.

Taylor, P. A., Walmsley, J. L., and Salmon, J. R.: 1983, 'A Simple Model of Neutrally Stratified Boundary Layer Flow over Real Terrain Incorporating Wavenumber-Dependent Scaling', *Boundary-Layer Meteorol.* **26**, 169–189.

Townsend, A. A.: 1965, 'The Response of a Turbulent Boundary Layer to Abrupt Changes in Surface Conditions', *J. Fluid Mech.* **22**, 799–822.

Townsend, A. A.: 1966, 'The Flow in a Turbulent Boundary Layer After a Change in Surface Roughness', *J. Fluid Mech.* **26**, 255–266.

Townsend, A. A.: 1972, 'Flow in a Deep Turbulent Boundary Layer over a Surface Distorted by Water Waves', *J. Fluid Mech.* **55**, 719–735.

Walmsley, J. L. and Salmon, J. R.: 1984, *A Boundary-Layer Model for Wind Flow over Hills: Comparison of Model Results with Askervein '83 Data*, Proc. European Wind Energy Conference and Exhibition, Hamburg, October 1984.

Walmsley, J. L., Salmon, J. R., and Taylor, P. A.: 1982, 'On the Application of a Model of Boundary-Layer Flow over Low Hills to Real Terrain', *Boundary-Layer Meteorol.* **23**, 17–46.

Walmsley, J. L., Taylor, P. A., and Keith, T.: 1986, 'A Simple Model of Neutrally Stratified Boundary-Layer Flow over Complex Terrain with Surface Roughness Modulations (MS3DJH/3R)', *Boundary-Layer Meteorol.* **36**, 157–186.

Zeman, O.: 1981, 'Progress in the Modelling of Planetary Boundary Layers', *Ann. Rev. Fluid Mech.* **13**, 253–272.

Zeman, O. and Jensen, N. O.: 1985, *Response of the Reynolds Stress Tensor to the Mean Flow Distortion over a Two-Dimensional Hill*, Seventh Symp. Turb. Diff., Amer. Meteorol. Soc., November 12–15, Boulder, Co.